

Yb₄LiGe₄ – A Yb Mixed Valent Zintl Phase with Strong Electronic Correlations

Sebastian C. Peter^{1*}, Steven M. Disseler², J. Niclas Svensson², Pietro Carretta³,
Michael J. Graf²

¹New Chemistry Unit, Jawaharlal Nehru Centre for Advanced Scientific Research, Jakkur,
Bangalore 560064, India

²Department of Physics, Boston College, Chestnut Hill, MA 02467 USA

³Department of Physics "A.Volta" and CNISM, University of Pavia, 27100 Pavia, Italy

Abstract

Single-phase samples of Yb₄LiGe₄ and Yb₅Ge₄ were synthesized using high frequency (HF) heat treatment. Yb₄LiGe₄ crystallizes in orthorhombic space group *Pnma* with the Gd₅Si₄ type of crystal structure and lattice parameters $a = 7.0571(1)$ Å, $b = 14.6239(1)$ Å, and $c = 7.6155(1)$ Å. One Yb position in Yb₅Ge₄ is substituted by the lithium atom and causes a distortion of the germanium tetragons in Yb₄LiGe₄. Investigation of the electronic state of Yb via magnetic susceptibility and X-ray absorption near-edge spectroscopy (XANES) revealed a presence of two electronic states of ytterbium, $4f^{13}$ and $4f^{14}$ (mixed valence), in Yb₅Ge₄ and Yb₄LiGe₄. Studies of the temperature dependence of the electrical resistivity, magnetization, ⁷Li spin-lattice relaxation rate and the specific heat indicate that strong electronic correlations are present in Yb₄LiGe₄, and below approximately 50 K there is a competition between ferromagnetic and antiferromagnetic correlations. Magnetic ordering in Yb₄LiGe₄, if present, occurs below the reported antiferromagnetic transition temperature of 1.7 K for Yb₅Ge₄.

PACS Numbers: 71.20.LP, 71.27.+a, 71.2d.+d

*Corresponding author. Phone: 080-22082298, Fax: 080-22082627
sebastiancp@jncasr.ac.in (S. C. Peter)

1. Introduction

Compounds with a general formula RE_5Tt_4 ($RE =$ Rare-earth; $Tt =$ Si, Ge) have been known for decades [1]. However, recently these materials captured the intense interest of the scientific community after the discovery of the giant magnetocaloric, magnetostriction and magnetoresistance effects in the Gd_5Si_4 - Gd_5Ge_4 system [2-9]. Pecharsky and co-workers demonstrated that the above mentioned physical properties can be tuned by the substitution of Ge with the isoelectronic Si in the $Gd_5(Si_xGe_{1-x})_4$ system [2-5, 7-9]. The family of $Gd_5Si_xGe_{4-x}$ alloys demonstrates a variety of unique physical phenomena related to magneto-structural transitions associated with reversible breaking and reforming of the interslab T_2 dimers that can be controlled by numerous external parameters such as chemical composition, magnetic field, temperature, and pressure. Similarly, the partial substitution of Ge by electron poorer Ga changes the valence electron count and affects the bond-making/breaking processes concomitant with the magnetic ordering [10]. These and other possibilities for exchanging Tt elements have been explored in the past. Interestingly, a different approach to tuning the material properties has been the substitution of the lanthanide metal with non magnetic element within the Gd_5Si_4 type structure, for example in $La_{5-x}Ca_xGe_4$ [11], $Ce_{5-x}Ca_xGe_4$ [11] and $Yb_{5-x}Mg_xGe_4$ [12] compounds.

Since Li is diagonally related to Mg and Yb_5Ge_4 exhibits mixed valent behavior, there exists the possibility for interchanging Li for either trivalent or divalent Yb. We have synthesized $Yb_{5-x}Li_xGe_4$ with the assumption that the compound may show a probable structural transformation and possibly interesting new physical properties. Several systems combining rare-earth elements with germanium and lithium have been studied [13-31]. Among these, the Yb-containing compounds have particular scientific interest because they can exhibit two energetically similar electronic configurations: the magnetic Yb^{3+} ($4f^{13}$) and the nonmagnetic Yb^{2+} ($4f^{14}$) one. Due to this feature Yb is usually considered as the “ f -hole” analogue of Ce. In this case, the roles of the $4f$ electron and $4f$ hole can be interchanged, and

many phenomena, such as intermediate valence, Kondo effect or heavy-fermion behavior, are observed in Ce and Yb analogues [32-35].

The crystal structure of RE_4LiGe_4 (RE = rare-earth metals) ternary compounds have been reported by *Pavlyuk et al* from the X-ray powder diffraction (XRPD) data [21]. A full crystal structure investigation has been performed from powder diffraction data for Tm_4LiGe_4 [21] and for Yb_4LiGe_4 ($Yb_2Li_{0.5}Ge_2$) using single crystal diffraction data [28]. Properties of Yb_4LiGe_4 have not yet reported.

In the paper, we report the synthesis of single-phase Yb_4LiGe_4 and Yb_5Ge_4 samples using a high frequency (HF) heat treatment method. Yb_5Ge_4 is a mixed valent system adopts Gd_5Si_4 type structure in orthorhombic space group $Pnma$. Yb_4LiGe_4 is a ternary variant of Yb_5Ge_4 substituting Li at one of the Yb position of Yb_5Ge_4 which further enhances the average valence of the Yb. Using high pressure we produced dense samples with well-defined dimensions and shape for measurements of physical properties like electrical and thermal transport and specific heat capacity. Because the band structure is highly sensitive to changes in the chemical bonding, we have carried out a broad characterization of electronic properties in the temperature range 1.8 K to 350 K employing X-ray absorption spectroscopy, heat capacity, DC and AC magnetic susceptibility, electrical resistivity, and NMR spectra and relaxation measurements. As shall be shown, these results provide clear evidence that Yb_4LiGe_4 is a strongly correlated system with competing magnetic interactions.

2. Experimental

The starting materials for the preparation of Yb_5Ge_4 and Yb_4LiGe_4 were ingots of ytterbium (99.99 wt%, Lamprecht), lithium rods (99.4 wt%, Alfa Aesar), and germanium pieces (99.9999 wt%, Chempur). The elements in stoichiometric ratios were heated in closed tantalum tubes to roughly 1070 K using a high frequency furnace. Careful handling of the ytterbium and lithium was necessary in order to minimize impurities, and was carried out inside an argon glove-box system. The synthesized samples were loaded into a planetary ball

mill (Pulverisette 7 Classic, Fritsch GmbH, Germany) for milling of about half an hour at a rotation speed of 600-800 rpm. In order to avoid excess heating of the vessels during milling, the process included equal pauses followed by active periods. The XRPD patterns of the samples obtained before and after milling were identical. Powder blends obtained from the milling process were then loaded again into Ta tubes and repeat the above process.

Phase analysis of both compounds was done by powder X-ray diffraction using a Guinier Huber G670 imaging plate camera applying Cu $K_{\alpha 1}$ radiation ($\lambda = 1.54056 \text{ \AA}$). The patterns were used to obtain the unit cell parameters by a least-squares refinement of the positions of the lines, calibrated by lanthanum hexaboride as an internal standard ($a = 4.1569 \text{ \AA}$).

Semi-quantitative microprobe analyses of the samples were performed with a Hitachi S-3400 scanning electron microscope (SEM) equipped with a PGT energy dispersive X-ray analyzer. Data were acquired with an accelerating voltage of 20 kV and a 60 s accumulation time. The EDS analysis taken on visibly clean surfaces of the samples gave the atomic composition close to 5:4 and 4:4 for Yb_5Ge_4 and Yb_4LiGe_4 , respectively.

The L_{III} X-ray absorption spectra (XAS) of Yb_5Ge_4 and Yb_4LiGe_4 were recorded in transmission arrangement at the EXAFS II beamline E4 of HASYLAB at DESY. Wavelength selection was realized by means of a Si (111) double crystal monochromator which yields an experimental resolution of approximately 2 eV (FWHM) for the experimental setup at the Yb L_{III} threshold of 8942 eV, and experiments were carried out in the energy range of 8829 eV to 9180 eV. Experimental data were measured using Yb_2O_3 as an external reference for the $4f^{13}$ configuration. Deconvolution of the XAS spectra was made by the program XASWin [36].

Measurements of the DC magnetization in applied magnetic fields between 10 mT and 7 T and in the temperature range 1.8 K - 400 K were carried out with a SQUID magnetometer (MPMS XL-7, Quantum Design). In addition, AC susceptibility measurements were made

using the Oxford MagLab platform on a second batch of Yb_4LiGe_4 samples, and confirmed the DC magnetization results presented here. Samples used for magnetic characterization were cut from disks produced by hot pressing of powder originally produced in a bulk form. Temperature-dependent magnetic susceptibility measurements of Yb_4LiGe_4 at 0.1 T show no difference from the powdered material, indicating a negligible inclusion of magnetic impurity phases.

The electrical resistivity measurements were performed on the same sample batch employing both DC and AC four-point methods in the temperature range 1.8 K - 300 K. The heat capacity was measured for $3 \text{ K} < T < 60 \text{ K}$ and in magnetic fields to 3 T using in the Oxford MagLab semi-adiabatic relaxation calorimeter platform. The heat capacity of the empty platform, which is less than 5% of the total heat capacity over the entire temperature range studied, was independently measured and subtracted off to obtain the sample specific heat.

^7Li NMR measurements were carried out on a TecMag Apollo spectrometer by using standard radiofrequency pulse sequences. The NMR spectra were obtained from the Fourier transform of half of the echo after a $\pi/2 - \tau - \pi$ pulse sequence. The characteristic decay time of the echo T_2 was measured at 300 K and 90 K, and found equal to $475 \mu\text{s}$ and $207 \mu\text{s}$, respectively. The spin-lattice relaxation rate $1/T_1$ was determined by following the recovery of nuclear magnetization after a saturating sequence of $\pi/2$ pulses. Data were taken in an applied magnetic field of 10 kG, with several additional points at 5 kG to demonstrate the relative insensitivity of the results to the field strength. The recovery law for the nuclear magnetization was found to be of the form

$$M = M_0 \left(1 - \exp \left[- (t / T_1)^\beta \right] \right),$$

that is, a stretched exponential, with a nearly temperature-independent exponent of $\beta = 0.9$. The deviation from a conventional exponential recovery law is likely to be due to the hyperfine coupling tensor anisotropy.

3. Results and discussion

3.1. Preparation

The Yb_4LiGe_4 sample after HF treatment is polycrystalline in nature, light grey with metallic luster and slightly air sensitive. The powder X-ray pattern of the first step synthesis reveals the presence of secondary phases ($\text{Yb}_3\text{Ge}_{4.3}$, Yb and Ge) in addition to Yb_4LiGe_4 . The main additional phase was identified as orthorhombic compound YbLiGe_2 [30] and was confirmed by EDX. The not completely reacted ytterbium and germanium may be present as elements and/or in form of $\text{Yb}_3\text{Ge}_{4.3}$, and may not have been detected by XRPD because of the complexity of the diffraction pattern. The first step material was then processed again by HF treatment and the resulting product was checked with X-ray diffraction and metallography. Only a single phase Yb_4LiGe_4 was observed within the detection limit of the X-ray diffractometer. The optical microscopy and the EDX results confirm the quality of the sample and reveal negligible amounts of elemental Ge as a secondary phase.

Single phase Yb_5Ge_4 was also synthesized by two step process. Initially we used a similar synthesis procedure as reported by Ahn *et al* [37]. The X-ray powder diffraction pattern of Yb_5Ge_4 sample after the first HF treatment showed mainly reflections of the orthorhombic crystal structure of the Gd_5Si_4 type. Small amounts of Yb_5Ge_3 and Ge were observed in the XRPD and in metallographic study. However, the sample obtained after second HF treatment was completely pure Yb_5Ge_4 as determined by XRPD.

The Guinier X-ray powder diffraction patterns were used to refine the unit cell parameters using lanthanum hexaboride as internal standard. The powder diffraction patterns of Yb_5Ge_4 and Yb_4LiGe_4 were indexed on the basis of the orthorhombic primitive cell with the space group $Pnma$. The lattice parameters are listed in Table 1. Whereas the lattice

parameters of Yb_5Ge_4 obtained in the present investigation are equal to the literature values within a few e.s.d. [37-40] the cell dimensions for our lithium-containing samples show some significant differences from the different literature data [37-40]. In all three cases, the lattice volume is smaller than that of Yb_5Ge_4 suggesting the successful implementation of Li into the initial crystal structure of the Gd_5Si_4 type. The marked variation of the lattice parameters in different studies indicates the differing levels of the Yb-by-Li substitution and, in fact, formation of the solid solution of Li in the binary ytterbium germanide - $\text{Yb}_{5-x}\text{Li}_x\text{Ge}_4$. Assuming that the Li content in the sample investigated in Ref. 28 agrees with $x = 1$, and applying Vegard's rule on the lattice volume, we conclude that the Li content in our sample is slightly smaller than 1 ($x \approx 0.94$).

3.2. Crystal structure

The simplest description of the parent compound Yb_5Ge_4 is given by the formula $[\text{Yb}_5]^{12+}[\text{Ge}_2]^{6-}[\text{Ge}_2]^{6-}$, and detailed studies of Yb_5Ge_4 [37-40] revealed mixed-valence behavior of ytterbium, and the formula can be written as $[\text{Yb}^{2+}]_{5-x}[\text{Yb}^{3+}]_x[\text{Ge}_2]^{6-}[\text{Ge}_2]^{6-}$. One position (Yb1) shows notably larger distances to the germanium ligands (first four shortest distances in the coordination sphere are 3.06, 3.14, 3.16 and 3.17 Å) if compared to the Yb2 position (the first four shortest distances are 2.86, 2.92, 2.92 and 2.93 Å). The third position (Yb3) reveals intermediate coordination behavior (2.96, 2.98, 2.98 and 3.17 Å) being rather closer to Yb2. The first site may be considered as a suitable for Yb^{2+} species, while the two others may support Yb^{3+} species. Yb1, Yb2 and Yb3 in Yb_5Ge_4 occupy at $8d$, $8d$ and $4c$ Wyckoff positions, respectively. Assuming that the formal charges for the germanium dumbbells are correct, this leads to the formula $[\text{Yb}^{2+}]_3[\text{Yb}^{3+}]_2[\text{Ge}_2]^{6-}[\text{Ge}_2]^{6-}$ [28]. These features open the possibility of changing of the electronic state of ytterbium and approaching the electron balance state by the substitution of the Yb atom in particular by a element with the lower formal charge (valence). One example of such a chemical modification by substitution of ytterbium by magnesium - $\text{Yb}_{5-x}\text{Mg}_x\text{Ge}_4$ - was recently reported [12]. Yb_4MgGe_4 has

alternating layers of Yb_2MgGe_2 and Yb_2Ge_2 along the b-direction, with a charge arrangement approximated by $(\text{Yb}^{2+})_2\text{Mg}^{2+}(\text{Ge}_2^{6-})$ and $(\text{Yb}^{3+})_2(\text{Ge}_2^{6-})$ following the Zintl Klemm concept [12, 28]. A consequence of substituting Li for Mg in this structure is that to maintain adequate charge balance, there should be either an increase in the average valence of the Yb in the Yb_2LiGe_2 pseudo-plane, or a slight undercharging of the Ge dimers leading to bond instabilities; our magnetic susceptibility measurements, presented below, indicate that the former explanation is correct. Here, magnesium substitution was observed on two positions Yb2 and Yb3, suggesting that the size but not the electronic factor is playing a more important role in this substitution chemistry. Using their crystal chemical analogy, lithium can be also used for replacement instead of magnesium. The presence of Li in the crystal structure was proved by Xie *et al* in their single crystal X-ray diffraction studies [28]. Since we haven't succeed to grow single crystals, we refined the crystal structure of Yb_4LiGe_4 from the powder diffraction data using full profile method [41], shown in Figure 1. The atomic coordinates obtained from our refinement are in very good agreement with the reported structure [28] (Tables 2 and 3). In agreement with the single crystal data, Yb_4LiGe_4 shows lithium substitution on the Yb3 position which has lower coordination number, and, thus, is suitable for the smaller lithium atoms. This finding reveals that the size ratio of the substituting atoms is more relevant for the formation of the solid solution $\text{Yb}_{5-x}\text{Li}_x\text{Ge}_4$, but not the formal charges derived from the interatomic distances as described above. It is also worth noting that because Li substitutes for Yb at the Yb3 position, this reduces the magnetic coupling between Yb^{3+} layers and potentially reducing the dimensionality of the system.

In order to shed light on the influence of lithium on the crystal structure of Yb_5Ge_4 it is worth comparing the different 2D segments in Yb_5Ge_4 and Yb_4LiGe_4 for $0.05 < y < 0.45$ (segment 1, Figures 2a and 2b) and for $-0.22 < y < 0.22$ (segment 2, Figures 2c and 2d). Segment 1 resembles the atomic arrangement in the structural motif of the FeB type (in the binary compound it has a composition ' Yb_2Ge_2 '), and segment 2 shows a pattern of the U_3Si_2

type (composition ‘Yb₃Ge₂’). The total composition may be obtained as Yb₂Ge₂ + Yb₃Ge₂ = Yb₅Ge₄. Different segments contain different [Ge₂]ⁿ⁻ species: segment 1 bears [Ge₂]⁶⁻ with a smaller Ge-Ge distance, segment 2 includes [Ge₂]⁶⁻ with a larger Ge-Ge distance. The lattice parameters of Yb₅Ge₄ are much larger than that of Yb₄LiGe₄ (see Table 2). This, of course, can be related to the fact that Yb is larger than Li. On the other hand, this leads to a slightly shorter Ge-Ge distances in Yb₄LiGe₄ (2.54 Å in segment 1 and 2.60 Å in segment 2) compared to those in Yb₅Ge₄ (2.57 Å in segment 1 and 2.65 Å in segment 2). Another striking feature after substituting the Yb₃ position with Li atom is the difference in angle between the Ge pairs in different segments. It remains very close in segment 2 with 32.11° and 32.75° for Yb₅Ge₄ and Yb₄LiGe₄, respectively. However, segment 1 shows a remarkable distortion after the substitution as it increased from 34.63° (Yb₅Ge₄) to 37.51° (Yb₄LiGe₄).

3.3. X-ray absorption spectroscopy (XAS)

The Yb- *L*_{III} spectra for Yb₄LiGe₄ and Yb₅Ge₄ (Figure 3) were fitted by XASWin[36] and display two peaks: one at 8948 eV associated with Yb³⁺ and the other at 8941 eV associated with Yb²⁺. The spectra of both compounds confirm the finding of mixed valence behavior. The evaluated average valence of the Yb atom is 2.57 in Yb₄LiGe₄ and 2.42 in Yb₅Ge₄, consistent with the mixed-valent state as inferred for Yb₅Ge₄ [37, 40]. The increase of the average valence of Yb with the lithium substitution is consistent with the electron balance formulation explained above, and confirmed by magnetic measurements, as described in Section 3.5.

3.4. Heat Capacity

In Figure 4 we show our results for the specific heat of Yb₄LiGe₄. The low-temperature increase and plateau near 3 K (shown in inset) are similar to the behavior observed in the parent compound Yb₅Ge₄ [37], and are attributed to magnetic degrees of freedom. Application of a magnetic field of 3 T has very little effect on the observed

behavior. The unusual temperature dependence will be discussed in Section 3.7 in the context of critical fluctuations as precursors to a magnetic phase transition.

3.5. Magnetic Susceptibility

At temperatures above 60 K the susceptibility of Yb_4LiGe_4 exhibits paramagnetic Curie-Weiss behavior $\chi = C/(T-\theta_p)$, where θ_p is Curie-Weiss temperature and C is a constant, as shown in Figure 5. From curve fits of the inverse susceptibility versus temperature we extracted a negative $\theta_p = -3(1)$ K, compared to -4 K reported for Yb_5Ge_4 [37] and consistent with antiferromagnetic correlations. The slope yielded an effective magnetic moment of $3.71(1) \mu_B$ per Yb, larger than the $2.72 \mu_B$ per Yb reported for Yb_5Ge_4 [37]. Following the analysis from Ref. 37, the fraction of Yb sites occupied by each valence state can be estimated from

$$\mu_{\text{eff}} = [n_{2+} (\mu_{2+})^2 + (1 - n_{2+}) (\mu_{3+})^2]^{1/2},$$

where μ_{2+} and μ_{3+} are the theoretical free magnetic moments of each valence state ($0 \mu_B$ and $4.54 \mu_B$, respectively), and n_{2+} is the fraction of Yb sites occupied by the non-magnetic Yb^{2+} . The result is an average value of $n_{2+} = 0.33(5)$.

First, we note that the estimated fraction of magnetic Yb^{3+} sites for Yb_4LiGe_4 $n_{3+} = 0.66$ is slightly larger than the 0.57 value extracted from the XAS measurements, and significantly larger than the value 0.36 reported for Yb_5Ge_4 [37]. This result is contrary to the expectation that Li would preferentially substitute for the smaller Yb^{3+} at the crystallographic $4c$ site, an inference consistent the quantum chemical calculations of Zhang and Miller [42] for Yb_4MgGe_4 . Rather, these results are again consistent with the proposal that an excess of electrons is required to stabilize the material, resulting in an increase in the average valency for the Yb ions.

Finally, we note that the Yb ions in Yb_5Ge_4 form a Shastry-Sutherland type lattice [43], as can be seen by comparing our Fig. 2b to Fig. 5a of Ref. 43, and so geometric

frustration effects could also play a role in the observed effective magnetic moment. It is interesting to speculate whether the lattice distortion created by Li substitution could in fact modify the degree of frustration thereby influencing the observed moment.

3.6. Electrical Resistivity

The room temperature resistivity is fairly large, roughly $1500 \mu\Omega\text{-cm}$, one to three orders of magnitude larger than the resistivity of ‘typical’ Yb-based intermetallic compounds. However, the sample remains a conductor down to 2 K, consistent with band structure calculations [28]. As shown in Figure 6, the resistivity is seen to increase sharply with decreasing temperature, but exhibits a broad maximum near 100 K, then increases very weakly upon further cooling. The behavior is qualitatively similar to that observed in strongly correlated Yb-systems with competing magnetic interactions [44, 45]. The inset to the figure shows a second small maximum near 10 K. Since no other properties show a structure at this temperature, which is well above the reported magnetic ordering temperature for Yb_5Ge_4 , we suggest, that this feature reflects a second energy scale to the electronic correlations in the system. However, we cannot rule out the possibility that the Yb oxidation states are varying with temperature, which could also contribute to the observed resistivity versus temperature curve.

3.7. ^7Li Solid State NMR

The temperature dependence of the spin-lattice relaxation rate $1/T_1$ (Figure 7) shows an unusual non-monotonic behavior, with $1/T_1$ increasing as temperature is lowered from 300 K, reaching a broad maximum located roughly near 60 K, and decreasing before attaining a nearly constant level near 4 K. This behavior is not typical of simple metals or of localized moment systems, but rather resembles behavior seen, for example, in the strongly correlated system the $\text{CeCu}_{6-x}\text{Au}_x$ system, where Kondo screening competes with the tendency towards magnetic ordering [46].

Fourier transforms of the T_1 pulse echo reveal a narrow line width of 10 kHz at 300 K, and which increases to about 250 kHz at 4 K; the low-temperature spectrum was confirmed using a point-by-point method. The line width varies nearly linearly with dc susceptibility χ (Figure 8) over the temperature range 300 K to 20 K. For a polycrystalline sample such as ours, the anisotropic hyperfine coupling will produce a distribution of resonance frequencies, and from the slope we estimate this anisotropic hyperfine coupling to be approximately 650 G, typical of dipolar coupling. It is interesting to notice that below about 20 K a deviation from the linear trend shown in Figure 8 is observed. This suggests a modification in the hyperfine coupling which might be associated with a change in the band structure. Assuming localized spins, the resulting exchange coupling is of order 5 K - 10 K, a value too large to be associated with purely dipolar coupling, and may be indicative rather of RKKY coupling of the Yb^{3+} ions. On the other hand, if we assume instead delocalized spins, 10 K represents the energy scale of correlations in the system. This latter interpretation is consistent with the observed maximum in the temperature-dependent resistivity and spin-lattice relaxation data. The results reported above show that Yb_4LiGe_4 share many properties with the Yb-based intermetallic compounds which are proximate to a magnetic ordering transition and can be tuned via substitution or pressure to exhibit non-Fermi liquid behavior [44, 45]. Following Moriya's theory for quantum fluctuations in the vicinity of a low-temperature magnetic transition [47], in Figure 9a we plot $1/T_1T$ versus dc susceptibility $\chi^{3/2}$ in the low temperature range $T < 30$ K, and find a linear variation; according to Ref. 38 this behavior is consistent with the presence of two-dimensional *ferromagnetic* fluctuations. In Figure 9b we plot C/T of Yb_4LiGe_4 versus $T^{-1/3}$ and find a linear behavior below 10 K, which is again consistent with Moriya's theory for a system exhibiting two-dimensional ferromagnetic fluctuations. This result seems highly unusual. While it is possible that the layered structure [12] of the material could produce two dimensional behavior (especially in light of the Li substitution at the Yb3 lattice position), the parent compound is reported to undergo *antiferromagnetic* ordering,

consistent with the negative Curie temperature extracted from our high temperature susceptibility results. A crossover from antiferromagnetic to ferromagnetic correlations has been also reported for Ce compounds on a Shastry-Sutherland lattice [43]. This crossover could occur around 10 K - 20 K where the change in the hyperfine coupling and the upturn in the resistivity are observed.

The inferred competition between Kondo screening of the local moments and RKKY interactions driving Yb_4LiGe_4 towards magnetic order, as well as the possible effects of magnetic frustration, make this material a likely candidate to exhibit unusual behaviors typically associated with competing order parameters, e.g., heavy fermion or quantum critical behavior. We are currently extending our measurements below 1.8 K to look for signatures of a strongly-correlated ground state, as well as to determine if the unusual critical behavior discussed above is related to a magnetic phase transition.

4. Concluding remarks

Single phase of Yb_5Ge_4 and Yb_4LiGe_4 were obtained by high frequency induction heating. Substitution of Li at Yb position in the Yb_2LiGe_2 pseudo-plane of parent compound Yb_5Ge_4 enhances the average valence of the Yb. X-ray absorption spectra in combination with the measurements of electrical conductivity and magnetic susceptibility on Yb_4LiGe_4 show presence of both Yb^{2+} and Yb^{3+} . Measurements of the electronic transport, nuclear spin-lattice relaxation, specific heat, and magnetization all point to the existence competing electronic interactions with multiple energy scales, and that the ground state may not be a simple antiferromagnet, as reported for the parent system Yb_5Ge_4 . The lack of conventional magnetic order would be consistent with the geometric frustration expected for the structure of the Yb sub-lattice, and with the mixed valence of the Yb ions.

Acknowledgements

This work was supported in part by National Science Foundation – Materials World Network grant DMR-0710525. The authors express their gratitude to the facilities at the EXAFS II beamline E4 of HASYLAB at DESY and U. Burkhardt for measurements.

Supporting Information Available. Powder XRD pattern of Yb₅G₄ and Yb₄LiGe₄.

References

1. P. Villars, L.D. Calvert, *Pearson's Handbook of Crystallographic Data for Intermetallic Compounds*. 2nd ed.; American Society for Metals: Materials Park: Ohio 44073, 1997.
2. K.A. Gschneidner, A.O. Pecharsky, V.K. Pecharsky, *J Appl Phys* 93 (2003) 4722-4728.
3. V.K. Pecharsky, K.A. Gschneidner, *Phys Rev Lett* 78 (1997) 4494-4497.
4. V.K. Pecharsky, K.A. Gschneidner, *Adv Cryog Eng* 43 (1998) 1729-1736.
5. V.K. Pecharsky, K.A. Gschneidner, *Adv Mater* 13 (2001) 683-686.
6. V.K. Pecharsky, A.P. Holm, K.A. Gschneidner, R. Rink, *Phys Rev Lett* 91 (2003) 197204.
7. V.K. Pecharsky, Y. Mudryk, D. Paudyal, K.A. Gschneidner, *Phys Rev B* 77 (2008) 024408.
8. V.K. Pecharsky, A.O. Pecharsky, K.A. Gschneidner, *J Alloy Compd* 344 (2002) 362-368.
9. Y. Mozharivskiy, A.O. Pecharsky, V.K. Pecharsky, G.J. Miller, *J Am Chem Soc* 127 (2005) 317-324.
10. Y. Mozharivskiy, W. Choe, A.O. Pecharsky, G.J. Miller, *J Am Chem Soc* 125 (2003) 15183.
11. L.-M. Wu, S. Kim, D.-K. Seo, *J. Am. Chem. Soc.* 127 (2005) 15682.
12. P.H. Tobash, S. Bobev, *J Am Chem Soc* 128 (2006) 3532-3533.
13. A. Czybulka, W. Schauerte, H.U. Schuster, *Z Anorg Allg Chem* 580 (1990) 45-49.
14. A. Czybulka, H.U. Schuster, *Z Naturforsch B* 34 (1979) 1234-1236.
15. A. Czybulka, G. Steinberg, H.U. Schuster, *Z Naturforsch B* 34 (1979) 1057-1058.
16. I. Grund, G. Zwiener, H.U. Schuster, *Z Anorg Allg Chem* 535 (1986) 7-12.
17. V.V. Pavlyuk, V.K. Belsky, O.I. Bodak, V.K. Pechersky, *Dopov Akad Nauk Ukr SSR B* (1987) 44-47.
18. V.V. Pavlyuk, O.I. Bodak, *Inorg Mater* 28 (1992) 877-879.
19. V.V. Pavlyuk, O.I. Bodak, *Russ Metall* (1993) 181-183.
20. V.V. Pavlyuk, O.I. Bodak, A.N. Sobolev, *Kristallografiya* 36 (1991) 880-882.
21. V.V. Pavlyuk, O.I. Bodak, V.E. Zavodnik, *Dopov Akad Nauk Ukr SSR B* (1990) 29-31.
22. V.V. Pavlyuk, V.K. Pecharskii, O.I. Bodak, *Kristallografiya* 33 (1988) 43-45.
23. V.V. Pavlyuk, V.K. Pecharskii, O.I. Bodak, V.A. Bruskov, *Kristallografiya* 33 (1988) 46-50.
24. V.V. Pavlyuk, V.K. Pecharskii, O.I. Bodak, A.N. Sobolev, *Russ Metall* (1989) 212-214.

25. V.V. Pavlyuk, V.K. Pecharsky, O.I. Bodak, *Dopov Akad Nauk Ukr SSR A* (1986) 76-78.
26. V.V. Pavlyuk, V.K. Pecharsky, O.I. Bodak, *Dopov Akad Nauk Ukr SSR B* (1989) 50-53.
27. V.V. Pavlyuk, V.K. Pecharsky, O.I. Bodak, V.A. Bruskov, *Kristallografiya* 32 (1987) 70-73.
28. Q.X. Xie, C. Kubata, M. Woerle, R. Nesper, *Z Anorg Allg Chem* 634 (2008) 2469-2476.
29. Q.X. Xie, R. Nesper, *Z Kristallogr-NCS* 219 (2004) 79-80.
30. Q.X. Xie, R. Nesper, *Z Kristallogr-NCS* 219 (2004) 81-82.
31. Q.X. Xie, R. Nesper, *Z Anorg Allg Chem* 632 (2006) 1743-1751.
32. K. AlamiYadri, D. Jaccard, *Solid State Communications* 100 (1996) 385-387.
33. K. Alami-Yadri, H. Wilhelm, D. Jaccard, *European Physical Journal B* 6 (1998) 5-11.
34. D. Jaccard, P. Link, E. Vargoz, K. AlamiYadri, *Physica B* 230 (1997) 297-300.
35. A. Kowalczyk, M. Falkowski, T. Tolinski, G. Chelkowska, *Solid State Communications* 139 (2006) 5-8.
36. L. Akselrud, Y. Grin, XASWIn Program, Max-Planck-Institut für Chemische Physik fester Stoffe: Dresden, 2004.
37. K. Ahn, A.O. Tsokol, Y. Mozharivskyj, K.A. Gschneidner, V.K. Pecharsky, *Phys Rev B* 72 (2005) 054404.
38. G. Balducci, S. Brutti, A. Cicciooli, G. Gigli, A. Palenzona, M. Pani, *J Phys Chem B* 111 (2007) 5132-5139.
39. M. Pani, A. Palenzona, *J Alloy Compd* 360 (2003) 151-161.
40. C.J. Voyer, D.H. Ryan, K. Ahn, K.A. Gschneidner, V.K. Pecharsky, *Phys Rev B* 73 (2006) 174422.
41. L. Akselrud, P.Y. Zavalii, Y.N. Grin, V.K. Pecharsky, B. Baumgartner, E. Wolfel, *Mater Sci Forum* 335 (1993) 133-136.
42. S. Misra, G.J. Miller, *J Am Chem Soc* 130 (2008) 13900-13911.
43. J.G. Sereni, M.G. Berisso, A. Braghta, G. Schmerber, J.P. Kappler, *Phys Rev B* 80 (2009) 024428.
44. E. Bauer, R. Hauser, L. Keller, P. Fischer, O. Trovarelli, J.G. Sereni, J.J. Rieger, G.R. Stewart, *Phys Rev B* 56 (1997) 711-718.
45. N. Papinutto, M.J. Graf, P. Carretta, A. Rigamonti, M. Giovannini, *Physica B* 359 (2005) 89-91.
46. E. Bauer, G. Hilscher, H. Michor, C. Paul, Y. Aoki, H. Sato, D.T. Adroja, J.G. Park, P. Bonville, C. Godart, J. Sereni, M. Giovannini, A. Saccone, *J Phys-Condens Mat* 17 (2005) S999-S1009.
47. A. Ishigaki, T. Moriya, *J Phys Soc Jpn* 67 (1998) 3924-3935.

Tables

Table 1. Lattice parameters of $\text{Yb}_{5-x}\text{Li}_x\text{Ge}_4$ ($x = 0, 1$).

Composition	a , Å	b , Å	c , Å	V , Å ³	Reference
Yb_5Ge_4	7.3430(9)	14.959(2)	7.829(1)	859.9(4)	this work
Yb_5Ge_4	7.342(2)	14.958(1)	7.828(1)	859.7	39
Yb_5Ge_4	7.3406(5)	14.9423(9)	7.8253(5)	858.3	37
Yb_4LiGe_4	7.0828(3)	14.6415(7)	7.6279(4)	791.0(3)	this work
Yb_4LiGe_4	7.0601(6)	14.628(1)	7.6160(7)	786.5	28
Yb_4LiGe_4	7.01	14.41	7.53	760.6	21

Table 2. Crystallographic data for Yb₄LiGe₄ obtained from this work compared with the reported single crystal data.

	Powder (this work)	Single Crystal
Mode of refinement	Full profile	Full matrix least squares on F ²
Space group, <i>Z</i>	<i>Pnma</i> , 4	<i>Pnma</i> , 4
Radiation, λ (Å)	Cu <i>K</i> α , 1.5406	Mo <i>K</i> α , 0.71073
Unit cell parameters		
<i>a</i> (Å)	7.0828(3)	7.060(1)
<i>b</i> (Å)	14.6415(7)	14.628(1)
<i>c</i> (Å)	7.6279(4)	7.616(1)
<i>V</i> (Å ³)	791.0(1)	786.5(1)
ρ_{calcd} (g/cm ³)	8.308	8.356
Reflections/parameters	1644/23	1599/44
Final R indices [<i>I</i> > 2 σ (<i>I</i>)]	<i>R</i> _i = 0.070	0.0302
	<i>R</i> _p = 0.140	0.0631

Table 3. Atomic coordinates and isotropic displacement parameters ($\text{\AA}^2 \times 10^3$) for Yb_4LiGe_4 . The single crystal data reported are added in italics.

Atom	Site	x	y	z	Ueq
Yb1	<i>8d</i>	0.01487(1)	0.09787(6)	0.18636(1)	8(1)
		<i>0.0147(1)</i>	<i>0.0598(1)</i>	<i>0.1859(1)</i>	<i>14(1)</i>
Yb2	<i>8d</i>	0.32746(1)	0.12653(7)	0.17319(1)	9(1)
		<i>0.3264(1)</i>	<i>0.1266(1)</i>	<i>0.1741(1)</i>	<i>13(1)</i>
Li	<i>4c</i>	0.0188(7)	0.25	0.505(6)	12(2)
		<i>0.0158(2)</i>	<i>0.25</i>	<i>0.519(2)</i>	<i>7(3)</i>
Ge1	<i>4c</i>	0.2821(4)	0.25	0.8676(4)	7(1)
		<i>0.2808(2)</i>	<i>0.25</i>	<i>0.8690(2)</i>	<i>14(1)</i>
Ge2	<i>4c</i>	0.0228(5)	0.25	0.0931(4)	12(1)
		<i>0.0181(2)</i>	<i>0.25</i>	<i>0.0959(2)</i>	<i>14(1)</i>
Ge3	<i>8d</i>	0.1632(4)	0.03655(1)	0.4664(3)	10(1)
		<i>0.1628(1)</i>	<i>0.0373(1)</i>	<i>0.4642(1)</i>	<i>15(1)</i>

Figures

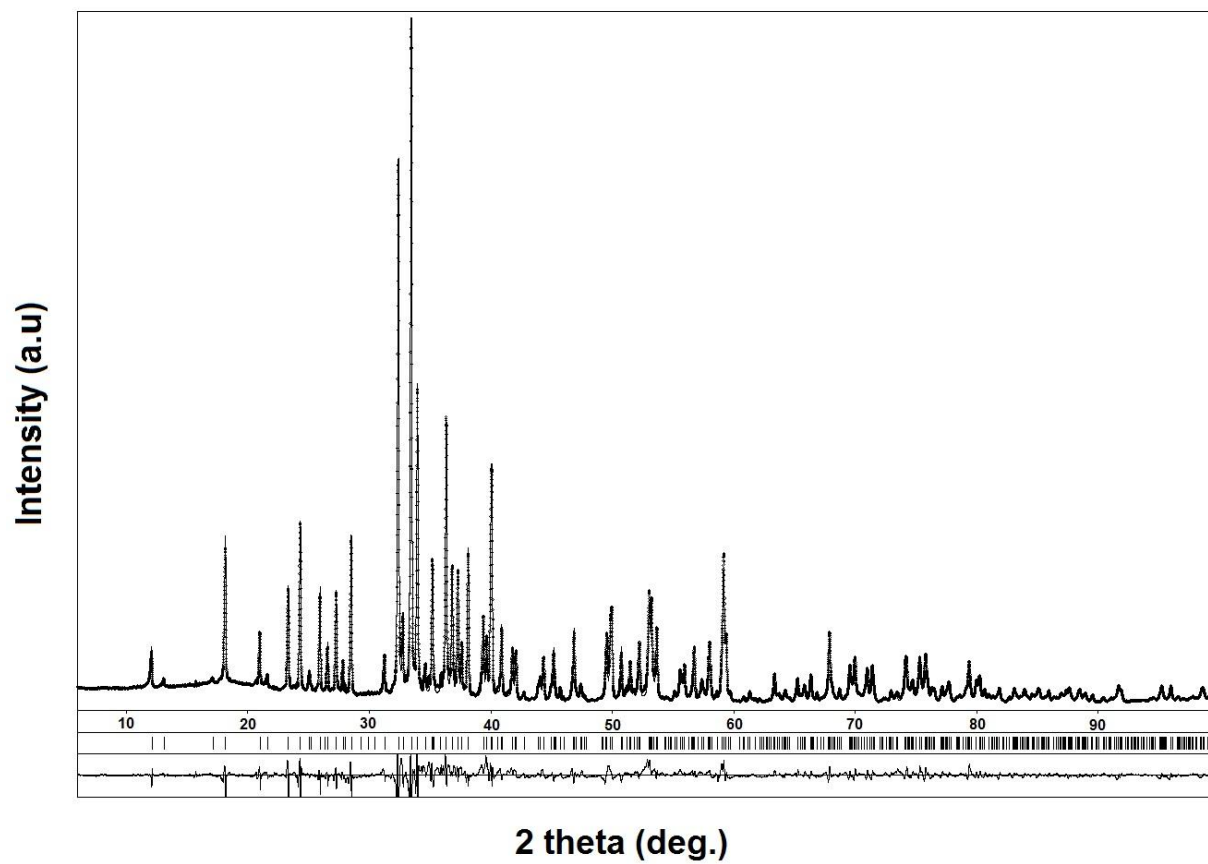


Figure 1. X-ray powder pattern measured at room temperature (+) and Reitveld fit (-) of Yb_4LiGe_4 .

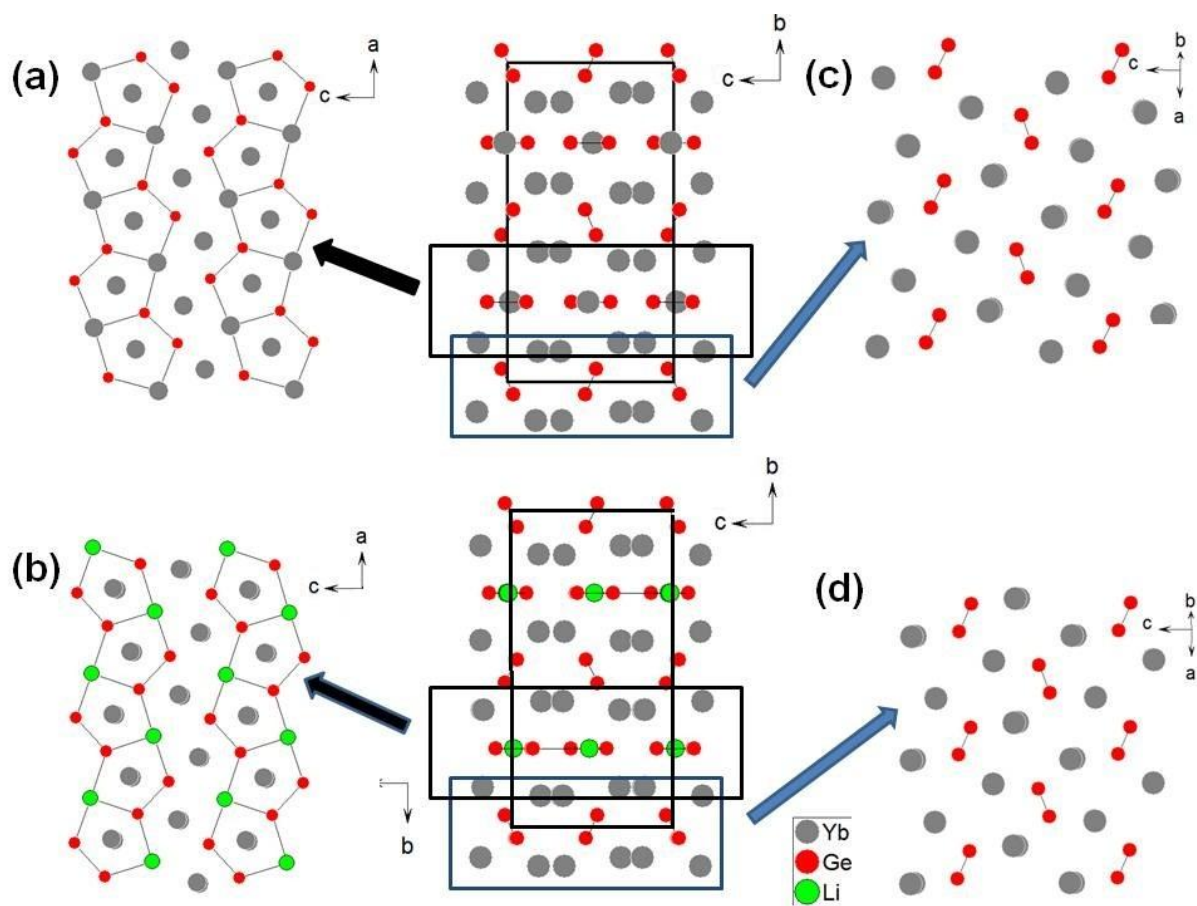


Figure 2. The two different segments of the crystal structures of Yb_5Ge_4 (top) and Yb_4LiGe_4 (bottom) within $0.05 < y < 0.45$ (a and b, segment 1) and $-0.22 < y < 0.22$ (c and d, segment 2).

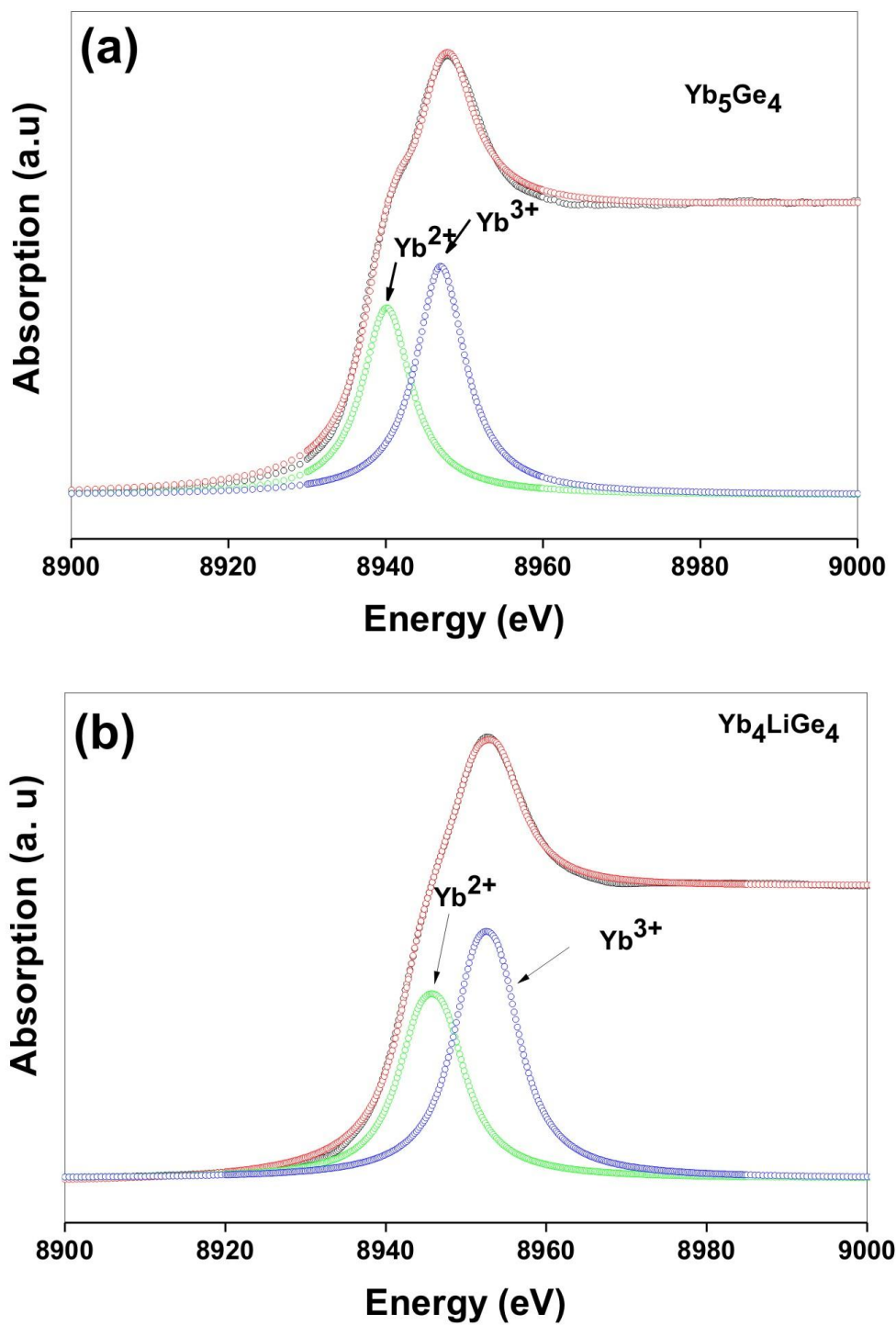


Figure 3. Yb-L_{III} X-ray absorption spectra at 300 K for Yb₅Ge₄ (a) and Yb₄LiGe₄ (b) are shown in red circles. The fitted curves for Yb²⁺ and Yb³⁺ are represented as green and blue circles, respectively.

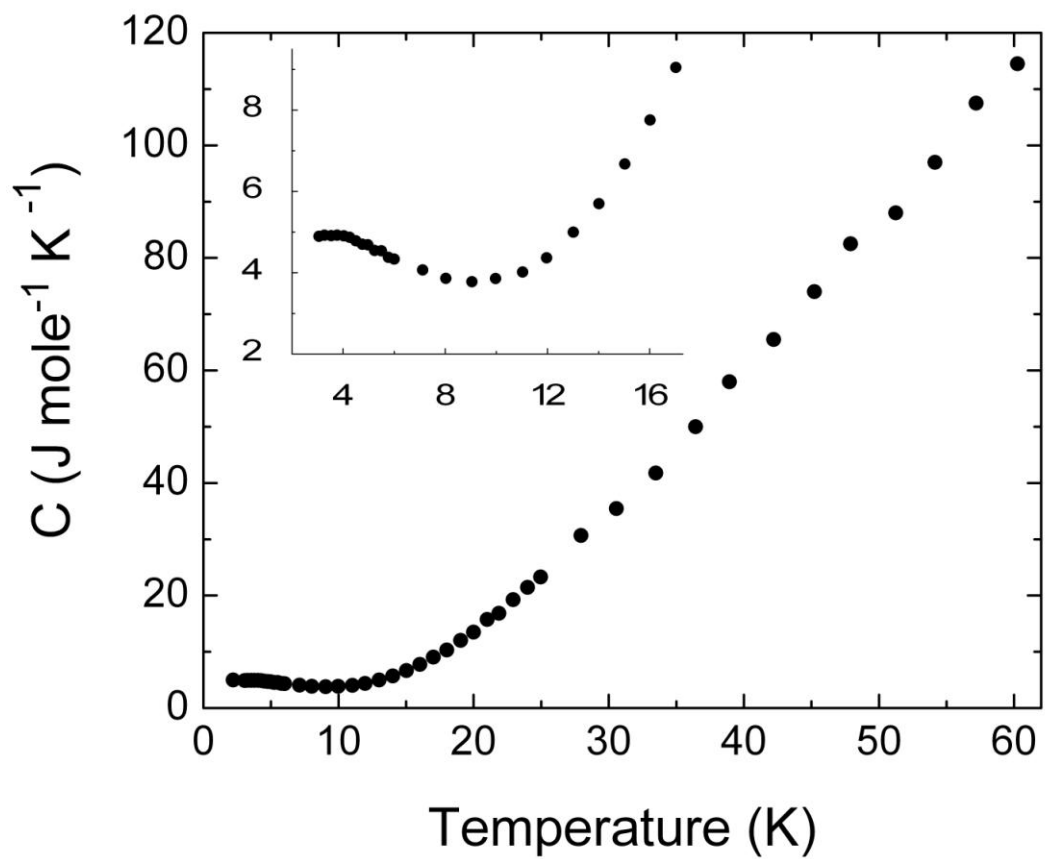


Figure 4. Specific heat of Yb_4LiGe_4 versus temperature. The low-temperature increase shown as plateau near 3 K in inset.

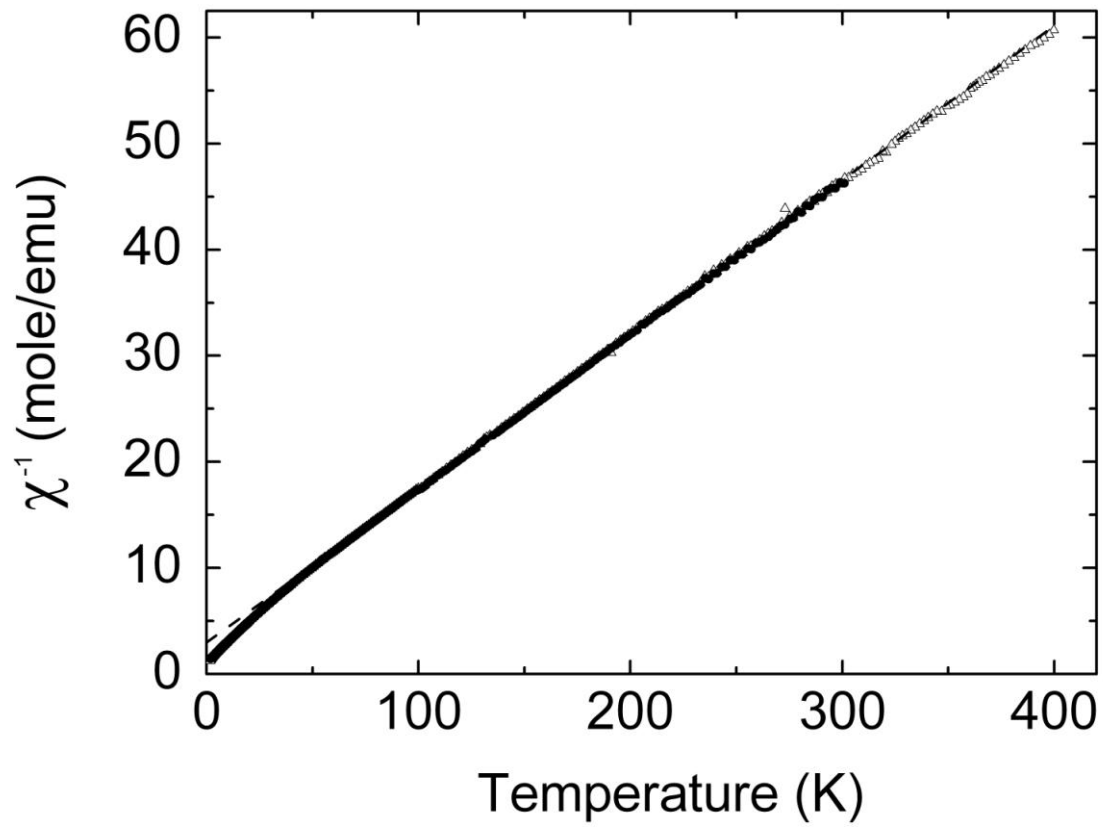


Figure 5. Inverse DC magnetic susceptibility of Yb_4LiGe_4 measured in fields of 1 kG and 10 kG versus temperature.

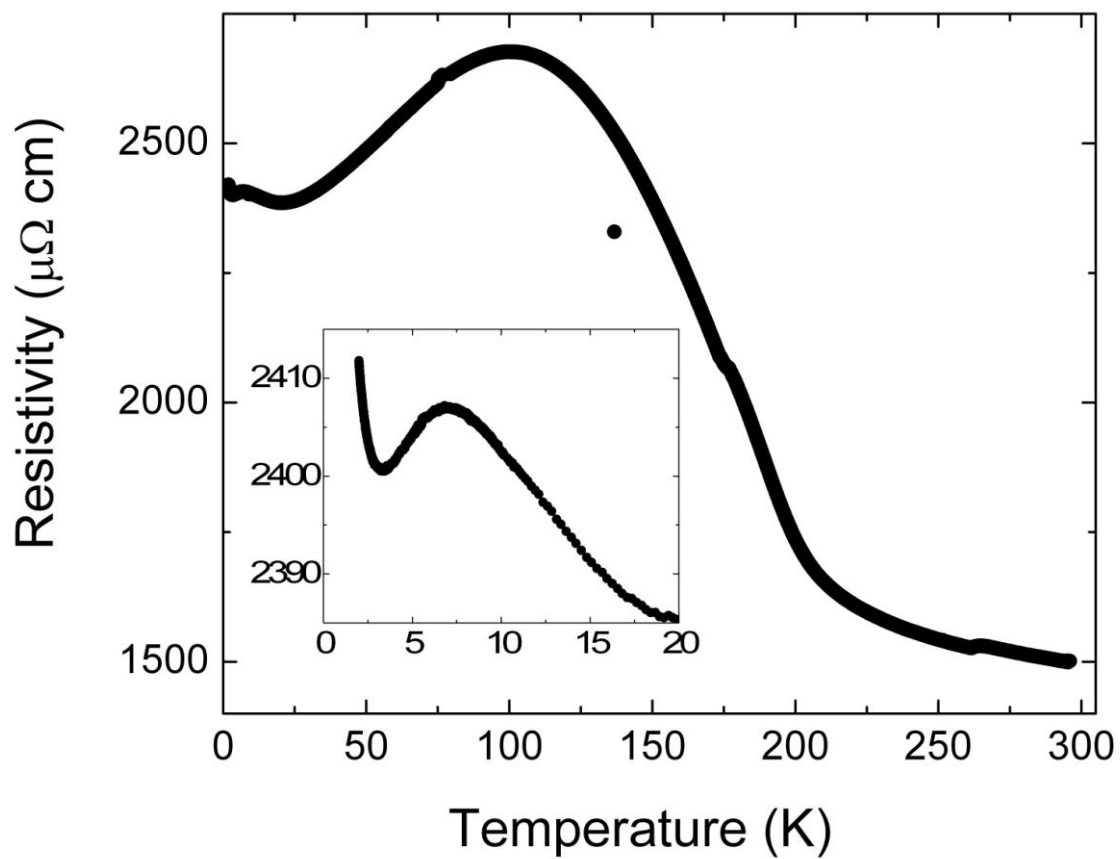


Figure 6. AC resistivity of Yb_4LiGe_4 versus temperature. The low temperature behavior is shown in the inset.

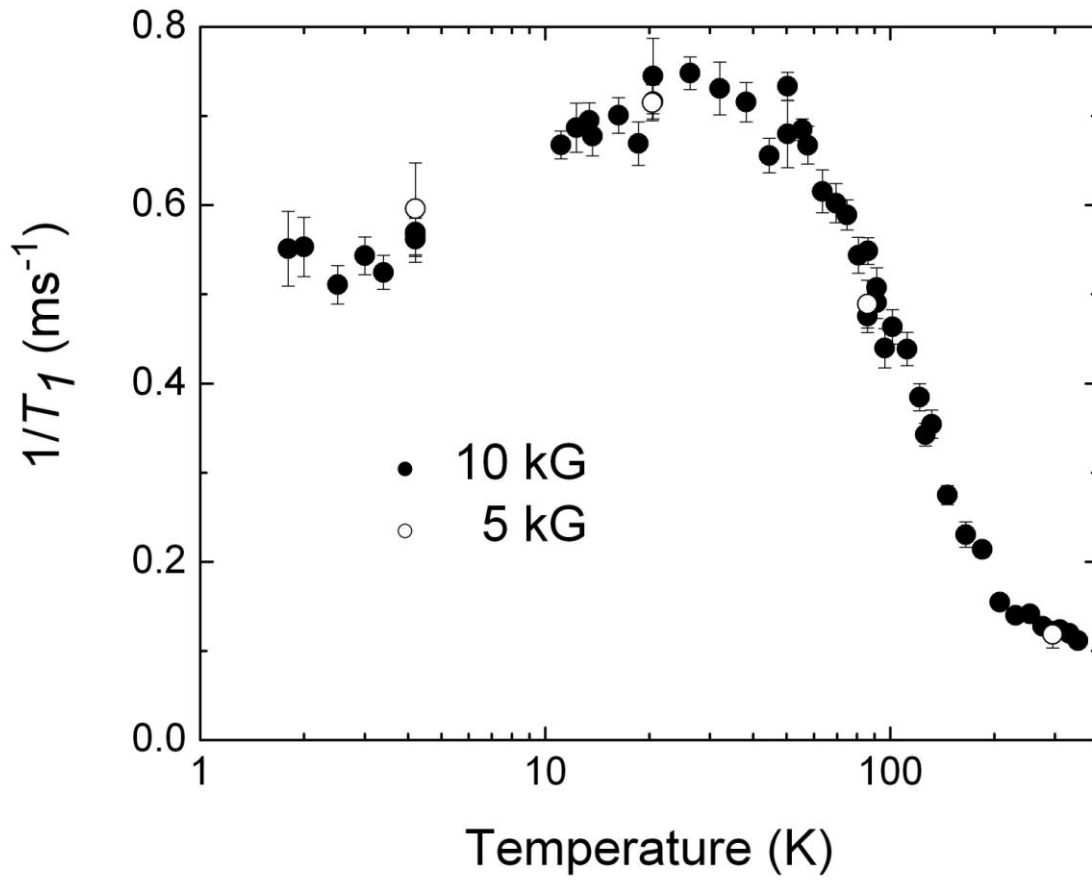


Figure 7. ${}^7\text{Li}$ spin-lattice relaxation rate of Yb_4LiGe_4 versus temperature.

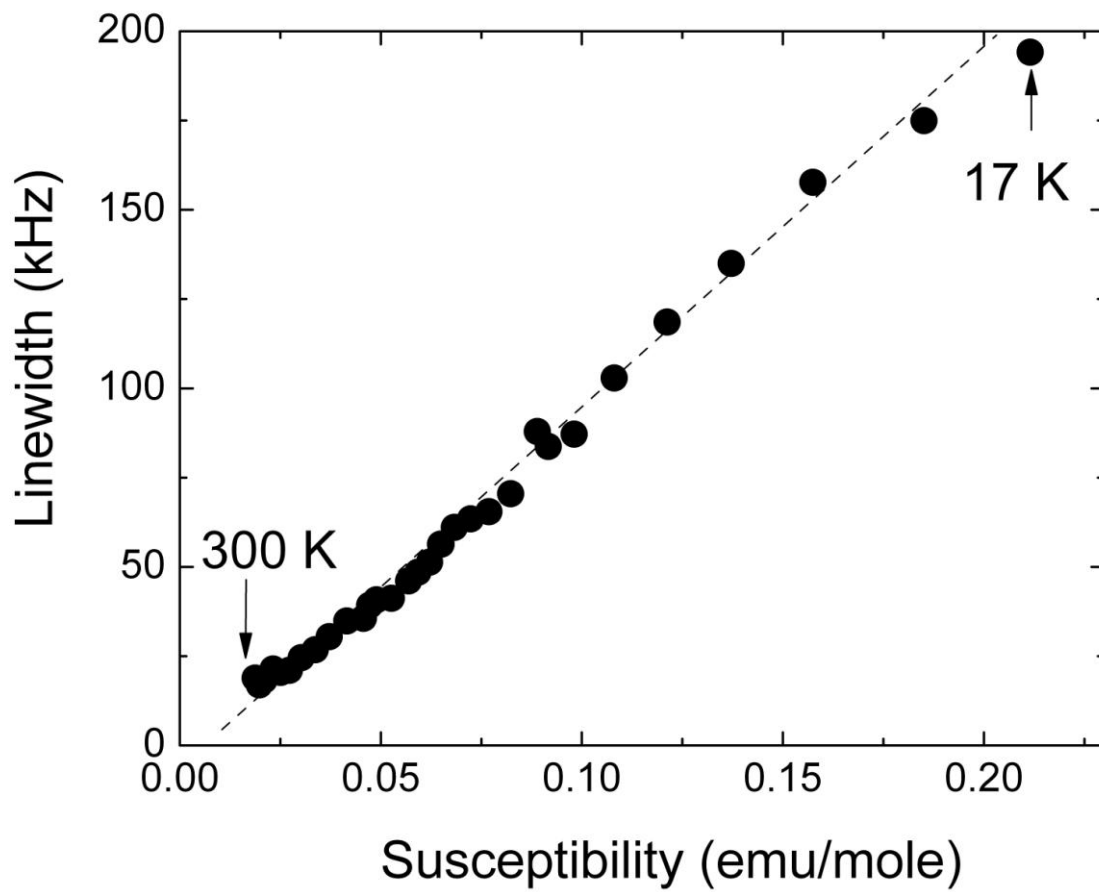


Figure 8. ${}^7\text{Li}$ line width of Yb_4LiGe_4 , obtained by Fourier transform of the pulse echo, plotted versus DC susceptibility in an applied magnetic field of 1 T.

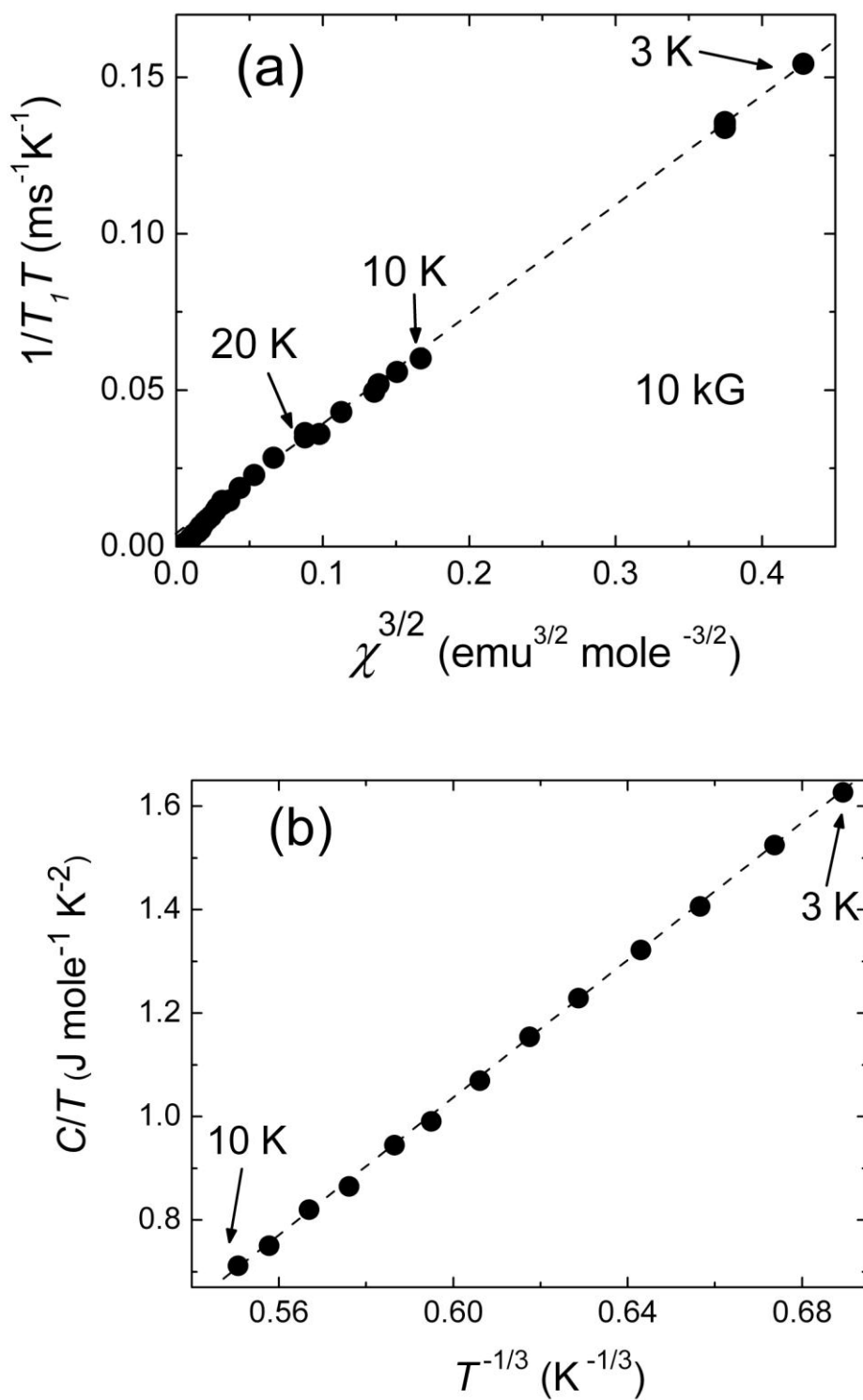


Figure 9. Analysis of the (a) ${}^7\text{Li}$ spin-lattice relaxation and (b) specific heat of Yb_4LiGe_4 , highlighting critical behavior which appears to follow the Ishigaki and Moriya prediction for two-dimensional system near to a low-temperature ferromagnetic phase transition described in Ref. 47.